Hybrid Finite Element and Volume Integral Methods for Scattering Using Parametric Geometry

John L. Volakis[1], Kubilay Sertel[1], Erik Jørgensen[2], and Rick W. Kindt[1]

Abstract: In this paper we address several topics relating to the development and implementation of volume integral and hybrid finite element methods for electromagnetic modeling. Comparisons of volume integral equation formulations with the finite element-boundary integral method are given in terms of accuracy and computing resources. We also discuss preconditioning and parallelization of the multilevel fast multipole method, and propose higher-order basis functions for curvilinear quadrilaterals and volumetric basis functions for curvilinear hexahedra. The latter have the desirable property of vanishing divergence within the element but non-zero curl. In addition, a new domain decomposition is introduced for solving array problems involving several million degrees of freedom. Three orders of magnitude CPU reduction is demonstrated for such applications.

keyword: Radar scattering, antenna radiation, magnetic materials, volume integral equations, finite-element boundary-integral method, fast multipole method, parallelization, preconditioning, curvilinear elements, higher-order basis functions.

1 Introduction

Electromagnetic scattering by inhomogeneous structures is of great interest in evaluating the overall scattering by modern composite vehicles. The same mathematical formulations are also suited for antennas, high frequency microwave circuits, electromagnetic coupling and interference, and inverse scattering applications. Thus, much interest exists in developing efficient formulations and numerical solutions in modeling volumetric scatterers having arbitrary permittivity (ε) and permeability (μ). In this paper we review some recent progress in modeling

volumetric scatterers with particular emphasis on materials having non-trivial permeability.

Initial efforts in modeling dielectric scatterers date back to the 1960s with J. H. Richmond, (1965) (see also A. F. Peterson, (1998) for a partial review of volume formulations) being among the first who published a numerical solution for the scattering by purely dielectric cylinders. Extensions to three dimensional scattering were carried out later by D. E. Livesay and K. Chen, (1974), D. H. Schaubert, D. R. Wilton, and A. W. Glisson, (1984), and R. D. Graglia, P. L. E. Uslenghi, and R. S. Zich, (1989). These solutions brought about the realization that practical size simulations of such targets were not possible using traditional integral equation solvers due to excessive $O(N^2)$ and $O(N^3)$ memory and CPU requirements, respectively. Thus, so far, applications of volume integral equations have been limited to electrically small and mostly purely dielectric structures.

During the 1990s, treatment of inhomogeneous scatterers focused on finite element (FE) methods and their hybrid finite element-boundary integral (FE-BI) counterparts [J. L. Volakis, T. Ozdemir, and J. Gong, (1997); J. L. Volakis, A. Chatterjee and L. Kempel, (1998)]. These were found attractive because of their geometrical and material adaptability coupled with their lower memory requirements. The introduction of fast integral methods [W. C. Chew, J.-M. Jin, E. Michielssen, and J. Song, ed., (2001), also see W. C. Chew, J. M. Song, T. J. Cui, S. Velamparambil, M. L. Hastriter, and B. Hu (2004)] prompted renewed interest in the solution of volume integral equations (VIEs) [J. L. Volakis, (1992)] for practical problem simulations. This interest is also motivated by the inherently fast convergence of VIE matrix systems as compared to corresponding systems generated via the FE-BI.

In this paper we consider volume integral and hybrid FE-BI formulations for scattering by inhomogeneous structures. In addition to the comparison of these for-

[1] ElectroScience Laboratory, The Ohio State University, 1320 Kinear Rd., 43212, Columbus, OH.
[2] Erik Jørgensen was at the University of Michigan. He is now at TICRA, Laederstraede 34 DK-1201 Copenhagen, DENMARK

mulations, several other unique features are covered in the paper. Specifically, we introduce three dimensional curvilinear elements for discretizing VIEs associated with inhomogeneous structures (essential for accurate modeling of high contrast dielectrics [J.-M. Jin, J. L. Volakis, and V. V. Liepa, (1989)]), multilevel fast multipole method (MLFMM) implementation of the associated systems, and related parallelization issues. Also, new hierarchical basis functions for improved convergence of the iterative solvers are introduced along with preconditioning techniques. Throughout the paper, emphasis is on the treatment of permeable dielectrics, and solutions are presented (for the first time) for three dimensional structures with non-trivial permeability.

2   Volume Integral Equation Formulation

To derive a general integral equation for inhomogeneous structures, we start with the VIE for an inhomogeneous dielectric structure in a source-free region given by [R. F. Harrington, (1968)]

$$\mathbf{E}(\mathbf{r}) = \mathbf{E}^{inc}(\mathbf{r}) + k_0^2 \int_v dv' \overline{\mathbf{G}}(\mathbf{r},\mathbf{r}') \cdot (\varepsilon_r(\mathbf{r}') - 1)\mathbf{E}(\mathbf{r}'). \quad (1)$$

In this, $\mathbf{E}^{inc}$ is the incident electric field or excitation, $\mathbf{E}$ is the total field within the domain (see Fig. 1), $k_0 = \omega\sqrt{\varepsilon_0\mu_0} = 2\pi/\lambda_0$ is the free-space wavenumber, $\varepsilon_r(\mathbf{r})$ is the relative dielectric constant of the inhomogeneous medium, and

$$\overline{\mathbf{G}}(\mathbf{r},\mathbf{r}') = \left[\overline{\mathbf{I}} + \frac{1}{k_0^2}\nabla\nabla\right] g(\mathbf{r},\mathbf{r}') \quad (2)$$

is the free-space dyadic Green's function with

$$g(\mathbf{r},\mathbf{r}') = \frac{e^{ik_0|\mathbf{r}-\mathbf{r}'|}}{|\mathbf{r}-\mathbf{r}'|} \quad (3)$$

(an $e^{-i\omega t}$ time convention is assumed and suppressed).

Numerical solution of this VIE has been given by several authors using various forms. D. E. Livesay and K. Chen, (1974) were the first to solve Eq. (1) using brick elements with piecewise constant expansions. Later D. H. Schaubert, D. R. Wilton, and A. W. Glisson, (1984) employed tetrahedra with linear basis functions, and R. D. Graglia, P. L. E. Uslenghi, and R. S. Zich, (1989) considered a moment method implementation of dielectric volumes using isoparametric elements.
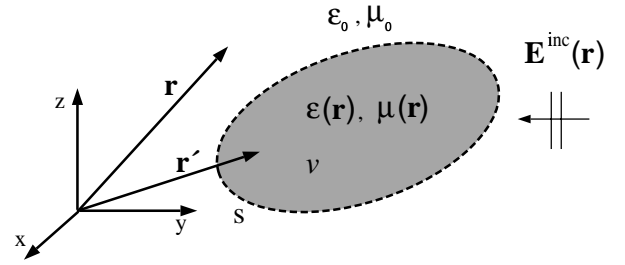

Figure 1 : Geometrical setup for VIE and FE-BI formulations

So far, simulations have been limited to small problems due to excessive memory and CPU requirements. Furthermore, all implementations were focused on non-magnetic volumes. However, for practical modeling of man-made structures, there is a requirement to allow for the presence of non-trivial permeability. Next, we introduce an integral equation for permeable structures which avoids surface integrals. To this end, we note that the dual of Eq. (1) is

$$\begin{aligned}\mathbf{H}(\mathbf{r}) &= \mathbf{H}^{inc}(\mathbf{r}) \\ &+ k_0^2 \int_v dv' \overline{\mathbf{G}}(\mathbf{r},\mathbf{r}') \cdot (\mu_r(\mathbf{r}') - 1)\mathbf{H}(\mathbf{r}')\end{aligned} \quad (4)$$

and since $\nabla \times \mathbf{E}(\mathbf{r}) = i\omega\mu(\mathbf{r})\mathbf{H}(\mathbf{r})$, it follows that the complete integral equation for general volumes is

$$\begin{aligned}\mathbf{E}(\mathbf{r}) &= \mathbf{E}^{inc}(\mathbf{r}) + k_0^2 \int_v dv' \overline{\mathbf{G}}(\mathbf{r},\mathbf{r}') \cdot (\varepsilon_r(\mathbf{r}') - 1)\mathbf{E}(\mathbf{r}') \\ &+ \int_v dv' \nabla' \times \overline{\mathbf{G}}(\mathbf{r},\mathbf{r}') \cdot (\mu_r(\mathbf{r}') - 1)\nabla' \times \mathbf{E}(\mathbf{r}').\end{aligned} \quad (5)$$

We note here that in contrast to the volume-surface integral equation given earlier [J. L. Volakis, (1992)], this representation does not involve any surface integrals. This integral equation is implemented below and validated for the first time using curvilinear elements. Below, we proceed to discretize the VIE with a general subdomain basis expansion. The specific curvilinear representation is given in the Appendix.

As usual, to discretize Eq. (5), we introduce the expansion

$$\mathbf{E}(\mathbf{r}) \approx \sum_{i=1}^{N} a_i \mathbf{e}_i(\mathbf{r}). \quad (6)$$

Substituting this into Eq. (5), and employing Galerkin's

testing gives the matrix system $\mathbf{Za} = \mathbf{b}$, where

$$
\begin{aligned}
Z_{ji} &= \langle \mathbf{e}_j(\mathbf{r}), \mathbf{e}_i(\mathbf{r}) \rangle \\
&\quad - \langle \mathbf{e}_j(\mathbf{r}), k_0^2 \int_v dv' \overline{\mathbf{G}}(\mathbf{r},\mathbf{r}') \cdot (\varepsilon_r(\mathbf{r}') - 1)\mathbf{e}_i(\mathbf{r}') \rangle \\
&\quad - \langle \mathbf{e}_j(\mathbf{r}), \int_v dv' \nabla' \times \overline{\mathbf{G}}(\mathbf{r},\mathbf{r}') \\
&\quad \cdot (\mu_r(\mathbf{r}') - 1)\nabla' \times \mathbf{e}_i(\mathbf{r}') \rangle
\end{aligned} \tag{7}
$$

and

$$
b_j = \langle \mathbf{e}_j(\mathbf{r}), \mathbf{E}^{inc}(\mathbf{r}) \rangle. \tag{8}
$$

The inner-product integrals over the source and testing domains appearing in Eq. (7) require a series of algebraic manipulations before they can be accurately implemented in a numerical solution. Specifically, for self-cell interactions careful numerical quadrature evaluation is necessary due to the singular nature of the Green's dyadic and its curl [K. Sertel and J. L. Volakis, (2002)]. For the first integral in Eq. (7), namely,

$$
\begin{aligned}
I_1 &= \langle \mathbf{e}_j(\mathbf{r}), k_0^2 \int_v dv' \overline{\mathbf{G}}(\mathbf{r},\mathbf{r}') \cdot (\varepsilon_r(\mathbf{r}') - 1)\mathbf{e}_i(\mathbf{r}') \rangle \\
&= \langle \mathbf{e}_j(\mathbf{r}), k_0^2 \int_v dv' (\overline{\mathbf{I}} + \frac{1}{k_0^2}\nabla\nabla g(\mathbf{r},\mathbf{r}')) \\
&\quad \cdot (\varepsilon_r(\mathbf{r}') - 1)\mathbf{e}_i(\mathbf{r}') \rangle
\end{aligned} \tag{9}
$$

it is necessary and customary to transfer one of the derivatives on the scalar Green's function to the testing function. This is accomplished through the divergence theorem as given in the Appendix of K. Sertel and J. L. Volakis, (2002). Evidently, for basis/testing functions having discontinuous normal components over adjacent elements, it is also necessary to evaluate the surface integral over element faces, appearing after the application of the divergence theorem [K. Sertel and J. L. Volakis, (2002)]. However, if the basis/testing functions are chosen to satisfy normal continuity, these surface integrals vanish (as discussed in D. H. Schaubert, D. R. Wilton, and A. W. Glisson, (1984)). The resulting integrals can be evaluated using the annihilation method (for general curvilinear coordinates), which converts first-order singular integrals into non-singular integrals for numerical integration as given in K. Sertel and J. L. Volakis, (2002).

We remark that the curl and divergence operations on the testing and basis functions imply use of at least linear expansion functions. For curvilinear brick elements (see Appendix), the divergence is more easily computed using covariant representations, whereas the curl is more easily computed using contravariant ones [A. F. Peterson and D. R. Wilton, (1996)]. Thus, care must be employed in whether a covariant or a contravariant form should be used. One approach is to employ a mix of these representations as is best suited for the evaluation of the various integrals.

3 Finite Element-Boundary Integral Equation Formulation

Finite element (FE) [J. L. Volakis, T. Ozdemir, and J. Gong, (1997); J. L. Volakis, A. Chatterjee and L. Kempel, (1998); J. L. Volakis, T. F. Eibert, and K. Sertel, (2000)] and finite element-boundary integral (FE-BI) methods have been among the workhorse techniques for frequency domain simulations over the past ten years. (also see P. Castillo, J. Koning, R. Rieben, and D. White, (2003) in this issue). Here, we present a brief overview for comparison with the VIE given above. The FE-BI is also presented from a general viewpoint as applied to non-planar structures [G. E. Antilla and N. G. Alexopoulos, (1994)] and is further optimized for large finite arrays.

In formulating the FEM, we begin with the functional

$$
\begin{aligned}
F(\mathbf{E}) &= \frac{1}{2} \int_v dv \left[\frac{1}{\mu_r}(\nabla \times \mathbf{E}) \cdot (\nabla \times \mathbf{E}) - k_0^2 \varepsilon_r \mathbf{E} \cdot \mathbf{E} \right] \\
&\quad - ik_0 Z_0 \int_s ds (\mathbf{E} \times \mathbf{H}) \cdot \hat{n}
\end{aligned} \tag{10}
$$

where the boundary integral S encloses the volume V (see Fig. 1). It is necessary to relate $\mathbf{E}$ and $\mathbf{H}$ on the surface to obtain a single functional in terms of $\mathbf{E}$ only. This is done by introducing the Stratton-Chu integral equation [A. J. Poggio, (1973)]. The electric field integral equation (EFIE) version of this is

$$
\Theta(\mathbf{J}) - \Omega(\mathbf{M}) = \mathbf{E}^{inc}, \tag{11}
$$

whereas the magnetic field integral equation (MFIE) has the form

$$
\Omega(\mathbf{J}) + \Theta(\mathbf{M}) = \mathbf{H}^{inc}, \tag{12}
$$

in which

$$\begin{aligned}
\Theta(\mathbf{X}) &= -ik_0 \int_s ds' \overline{\mathbf{G}}(\mathbf{r},\mathbf{r}') \cdot \mathbf{X}(\mathbf{r}') \\
&= -ik_0 \int_s ds' g(\mathbf{r},\mathbf{r}') \mathbf{X}(\mathbf{r}') \\
&\quad + \frac{i}{k_0} \int_s ds' \nabla g(\mathbf{r},\mathbf{r}') \nabla' \cdot \mathbf{X}(\mathbf{r}') \quad (13) \\
\Omega(\mathbf{X}) &= T\mathbf{Y}(\mathbf{r}) + \oint_s ds' \mathbf{X}(\mathbf{r}') \times \nabla g(\mathbf{r},\mathbf{r}')
\end{aligned}$$

with $\mathbf{Y} = -\hat{n} \times \mathbf{X}$, $T = 1 - \beta/4\pi$, and $\hat{n}$ denoting the unit normal to the bounding surface ($\beta = 2\pi$ for a smooth surface). Typically, a linear combination of the two formulations, referred to as the combined field integral equation (CFIE) is employed to avoid resonance difficulties and poor conditioning.

The electric field is solved from Eq. (10) by setting $\partial F(\mathbf{E})/\partial \mathbf{E} = 0$ and on discretizing the resulting equations using the appropriate expansion [G. E. Antilla and N. G. Alexopoulos, (1994)] results in the system

$$\begin{bmatrix} \mathbf{E_{vv}} & \mathbf{E_{vs}} & 0 \\ \mathbf{E_{sv}} & \mathbf{E_{ss}} & \mathbf{B} \\ 0 & \mathbf{P} & \mathbf{Q} \end{bmatrix} \begin{bmatrix} \mathbf{E_v} \\ \mathbf{E_s} \\ \mathbf{H_s} \end{bmatrix} = \begin{bmatrix} 0 \\ 0 \\ \mathbf{b} \end{bmatrix} \quad (14)$$

where the element matrices are given by

$$\begin{aligned}
P_{ji} &= -\alpha \int_s ds \, \mathbf{t}_j \cdot \Omega(\mathbf{e}_i) \\
&\quad + (1-\alpha) \int_s ds \, \hat{n} \times \mathbf{t}_j \cdot \Theta(\mathbf{e}_i) \\
Q_{ji} &= \alpha \int_s ds \, \mathbf{t}_j \cdot \Theta(\mathbf{e}_i) + (1-\alpha) \int_s ds \, \hat{n} \times \mathbf{t}_j \cdot \Omega(\mathbf{e}_i) \\
b_j &= \alpha \int_s ds \, \mathbf{t}_j \cdot \mathbf{E}^{inc} + (1-\alpha) \int_s ds \, \hat{n} \times \mathbf{t}_j \cdot \mathbf{H}^{inc} \quad (15)
\end{aligned}$$

with $\mathbf{e}_i$ and $\mathbf{t}_j$ being the expansion and testing functions for the surface quantities, respectively, and α is a scale factor chosen from zero to unity.

For a general inhomogeneous structure consisting of material and conducting components, the resulting system in Eq. (14) is highly heteregeneous, consisting of a sparse FE part (**E** and **B** submatrices in Eq. (14)) and a full integral equation part (**P** and **Q** submatrices in Eq. (14)). In practice, this highly heteregeneous FE-BI system may result in a poorly convergent iterative solution, especially for large scale simulations. Since the application of fast methods (such as the MLFMM) implies use of iterative solvers, this poor convergence behavior introduces a bottleneck in terms of total solution

time, especially for multi-spectral simulations. Preconditioning methods may therefore be necessary for certain problems to achieve convergence (see R. D. Graglia, P. L. E. Uslenghi, and R. S. Zich, (1989); J.-M. Jin, J. L. Volakis, and V. V. Liepa, (1989); G. E. Antilla and N. G. Alexopoulos, (1994) and for higher-order basis functions see R. D. Graglia, D. R. Wilton, and A. F. Peterson, (1997); B. M. Kolundzija and B. Popovic, (1993); J. P. Webb, (1999)). Clearly, it is important to use preconditioners which can be implemented in favorable CPU times. Among them, the ILU [K. Sertel and J. L. Volakis, (2000)] and block-diagonal [Y. Saad, (1996)] preconditioners have been found quite effective. In modeling layered geometries, substantial improvement in matrix condition can be achieved by choosing hexahedral elements rather than the usual tetrahedra. Curvilinear elements also allow for geometrical modeling fidelity and have been shown to be very effective for antenna arrays [R. W. Kindt, K. Sertel, E. Topsakal, and J. L. Volakis, (2003)] as well as scattering applications [R. D. Graglia, P. L. E. Uslenghi, and R. S. Zich, (1989)].

When dealing with arrays, certain advantages associated with the repeatability of each array element can be exploited. More specifically, we observe from Fig. 2 that each element has identical geometry and thus the FE-BI matrix system takes the form

$$\begin{bmatrix} \mathbf{a}_{11} & \mathbf{a}_{12} & \dots & \mathbf{a}_{1M} \\ \mathbf{a}_{21} & \mathbf{a}_{22} & \dots & \mathbf{a}_{2M} \\ \vdots & \vdots & \ddots & \vdots \\ \mathbf{a}_{M1} & \mathbf{a}_{M2} & \dots & \mathbf{a}_{MM} \end{bmatrix} \begin{Bmatrix} \mathbf{x}_1 \\ \mathbf{x}_2 \\ \vdots \\ \mathbf{x}_M \end{Bmatrix} = \begin{Bmatrix} \mathbf{b}_1 \\ \mathbf{b}_2 \\ \vdots \\ \mathbf{b}_M \end{Bmatrix} \quad (16)$$

where the sub-matrices $\mathbf{a}_{mm'}$ denote the individual coupling operators between the m and m' elements in the array, $\{\mathbf{x}_1, \dots, \mathbf{x}_M\}^T$ is a block-vector containing the unknown vectors for each array element, and $\{\mathbf{b}_1, \dots, \mathbf{b}_M\}^T$ is also a block-vector providing the excitations on the array elements. Each of the diagonal submatrices is of the same form as given in Eq. (14), whereas the off-diagonal submatrices matrices describe the coupling among the m and m' array elements (see Fig. 2). If we use a boundary integral to enclose the volume of each array element, then all off-diagonal submatrices will just contain the **P** and **Q** submatrices in Eq. (14).

Of importance is that the coupling submatrices only depend on the absolute distance among elements and
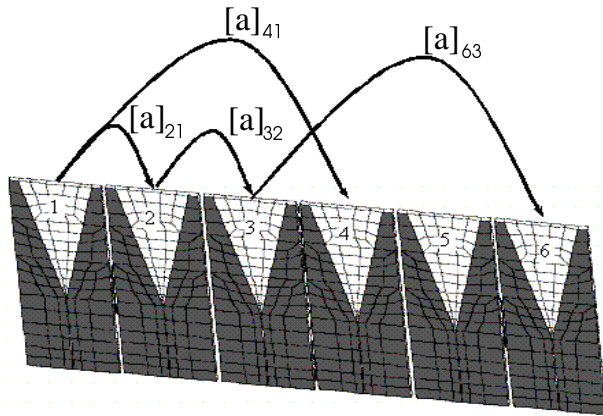
Figure 2 : Illustration of redundant coupling paths in a 1×6 array.

the diagonal submatrices are identical. Consequently, the overall matrix in Eq. (16) is block Toeplitz. Thus, Eq. (16) can be cast in the circulant form $\Pi *\{\mathbf{x}\} = \{\mathbf{b}\}$ where "$*$" implies convolution and $\Pi = \{\mathbf{a}_{M-1}, \ldots, \mathbf{a}_1, \mathbf{a}_0, \mathbf{a}_{-1}, \ldots, \mathbf{a}_{1-M}\}$ in which the notation $\mathbf{a}_{mm'} = \mathbf{a}_{m-m'} = \mathbf{a}_p$ has been introduced. This observation implies that the fast Fourier transform (FFT) can be employed to carry out the matrix-vector products of the entire FE-BI system in $O(N \log N)$ CPU time and using $O(N)$ storage, where $N = m^2 M$.

In addition to the above, we may further exploit the fact that all diagonal submatrices, i.e. $\mathbf{a}_{mm'} = \mathbf{a}_{m-m'} = \mathbf{a}_p$ for $p = 0$, are identical, and use the inverse of $\mathbf{a}_0$ to precondition the entire matrix system. This type of preconditioning has been found very effective once the overall FE-BI matrix is re-structured as suggested in Eq. (16). Details of this decomposition method can be found in R. W. Kindt, K. Sertel, E. Topsakal, and J. L. Volakis, (2003).

In closing this section, we note that the MLFMM can be readily incorporated into the FE-BI method to speed-up the solve time associated with large scattering and/or radiation problems having arbitrary shape. The MLFMM (already used for perfectly conducting targets) can be extended to both VIE and FE-BI methods by merely incorporating the signature functions into their respective algorithms. Specifically, for the FE-BI method, since the same basis functions are used for both surface unknowns ($\mathbf{E}_s$ and $\mathbf{H}_s$), the same signature functions can be utilized for both. Also, the clustering of the surface unknowns is based solely on the surface magnetic field

and thus the same clustering can be used for the surface electric field unknowns, leading to significant memory savings.

A detailed discussion on the FFT acceleration for antenna arrays and the MLFMM implementation for the VIE and FE-BI systems is beyond the scope of this paper. However, several performance analyses and results are provided in the subsequent sections.

4 Higher-order Basis Functions

As mentioned above, some key issues related to the efficient and accurate modeling of large scale structures are the discretization accuracy, error propagation and convergence of the iterative algorithms. Use of curvilinear elements allow for body conforming modeling. Thus, much fewer elements need be used to achieve the same accuracy. Fewer discretization elements also imply improvement in the condition number, leading to improved convergence. This is demonstrated in Tab. 1 which refers to a PEC sphere (the MLFMM was used to carry out the solution using linear conformal basis functions on quadrilateral surface patches). As can be observed, the same problem at the same frequency can be solved using 3.5 samples per λ in 10.1 s. per iteration vs. 38.4 s. per iteration if 10 samples per λ is used to still maintain acceptable error.

Table 1 : Convergence rates with different mesh densities.

Discretization	Number of Iterations	Time per Iteration(s.)	Solution time(s.)
$3.5/\lambda$	21	10.1	212.3
$10/\lambda$	–	38.4	–

A natural need in using larger elements is the employment of higher-order bases. Such bases have been extensively examined [R. D. Graglia, D. R. Wilton, and A. F. Peterson, (1997); B. M. Kolundzija and B. Popovic, (1993); J. P. Webb, (1999); L. S. Andersen and J. L. Volakis, (1999)] and can be categorized as either interpolatory or hierarchical. The latter are more attractive since they allow for using different order expansions at each element (surface or volume) of the discretized body. However, such higher-order bases may often lead to substantial deterioration in convergence. To improve convergence, we must improve the orthogonality of these

elements while still maintaining their hierarchality. Below, we introduce such an expansion.

Without loss of generality, let us consider the quadrilateral patch defined in the local curvilinear (u, v) coordinate system, where $0 \leq u, v \leq 1$. The patch can be bilinear, biquadratic, or even higher-order as determined by the position vector $\mathbf{r}(u, v)$ defining the patch surface. The surface current on the patch is expanded as $\mathbf{J}_s = J_{su}\mathbf{a}_u + J_{sv}\mathbf{a}_v$, where $\mathbf{a}_u$ and $\mathbf{a}_v$ are the covariant unitary vectors $\mathbf{a}_u = \frac{\partial \mathbf{r}}{\partial u}$ and $\mathbf{a}_v = \frac{\partial \mathbf{r}}{\partial v}$. Instead of the hierarchical expansion (only the u-directed currents are considered) introduced by B. M. Kolundzija and B. Popovic, (1993)

$$
\begin{aligned}
J_{su} &= \frac{1}{A} \sum_{n=0}^{N} \{ c_{0n}(1 - (2u - 1)) \\
&+ c_{1n}(1 + (2u - 1)) \} (2v - 1)^n \\
&+ \frac{1}{A} \sum_{n=0}^{N} \left\{ \sum_{\substack{m=2 \\ m \text{ even}}}^{M} c_{mn}((2u - 1)^m - 1) \right. \\
&+ \left. \sum_{\substack{m=3 \\ m \text{ odd}}}^{M} c_{mn}((2u - 1)^m - (2u - 1)) \right\}
\end{aligned} \tag{17}
$$

where c_{mn} are the constants of the expansion and $A = |\mathbf{a}_u \times \mathbf{a}_v|$, we propose the alternative expansion [E. Jorgensen, J. L. Volakis, P. Meincke, and O. Breinbjerg, (2002)] (also polynomial)

$$
\begin{aligned}
J_{su} &= \frac{1}{A} \sqrt{\frac{3}{8}} \sum_{n=0}^{N} [b_{0n}(1 - (2u - 1)) \\
&+ b_{1n}(1 + (2u - 1))] C_n^v P_n(2v - 1) \\
&+ \frac{1}{A} \sum_{m=2}^{M} \sum_{n=0}^{N} b_{mn} C_m^u [P_m(2u - 1) \\
&- P_{m-2}(2u - 1)] C_n^v P_n(2v - 1)
\end{aligned} \tag{18}
$$

where $P_n(v)$ are the Legendre polynomials given by $P_n(v) = \frac{1}{2^n n!} \frac{d^n}{dv^n}(v^2 - 1)^n$ and b_{mn} are the new expansion coefficients. The constants $C_m^u = \sqrt{\frac{(2m-3)(2m+1)}{2(2m-1)}}$ and $C_n^v = \sqrt{2n+1}$ are scaling factors chosen such that the Euclidian norm of each basis function is unity on a unit square patch. It is important to note that the polynomials $1 - (2u - 1)$, $1 + (2u - 1)$, $P_2(2u - 1) - P_0(2u - 1)$, ..., $P_M(2u - 1) - P_{M-2}(2u - 1)$, can be shown to span the space of polynomials of degree M. Also, since the first two terms are non-zero at $u = 0$ or $u = 1$, they must

be matched with corresponding functions on the neighboring patches to enforce continuity of the normal current component.

Although similar to the expansion in Eq. (17), the basis in Eq. (18) differs in three important ways. First, orthogonal polynomials are used. Second, the continuity equation is incorporated by modifying the polynomials in a way that preserves orthogonality as much as possible, and third, a scaling factor is included to improve the condition number. The interpolatory bases of R. D. Graglia, D. R. Wilton, and A. F. Peterson, (1997) are limited to a fixed approximation order corresponding to the choice $N = M - 1$. In this special case, all three bases (those in R. D. Graglia, D. R. Wilton, and A. F. Peterson, (1997); B. M. Kolundzija and B. Popovic, (1993) and Eq. (18)) span the same polynomial space, have the same number of unknowns in a single patch, and have the same number of unknowns associated with two patches. Consequently, the current obtained via the moment method will be identical for all three bases, although the implementation and condition number of the resulting matrix may differ significantly. To demonstrate the improved condition number of the new basis defined in Eq. (18), let us consider the scattering by a pair of parallel PEC plates solved via the EFIE. Fig. 3 shows the matrix condition number obtained with the bases in [R. D. Graglia, D. R. Wilton, and A. F. Peterson, (1997); B. M. Kolundzija and B. Popovic, (1993)] and those in Eq. (18). As seen (the annihilation technique in K. Sertel and J. L. Volakis, (2002) was used for the self-cells), the condition number appears to be exponentially increasing as the order of the hierarchical bases in B. M. Kolundzija and B. Popovic, (1993) increase, but remains fairly constant for our proposed hierarchical bases given by Eq. (18). This is important since large physical elements can be used with higher-order expansion without adverse effects on the system convergence.

5 MLFMM on Parallel Architectures

The most CPU intensive component in any iterative solution of a dense matrix system is the execution of the matrix-vector product $\mathbf{Za}$ mentioned earlier. This is usually an $O(N^2)$ operation which can be reduced to $O(N \log N)$ via the MLFMM procedure [W. C. Chew, J.-M. Jin, E. Michielssen, and J. Song, ed., (2001); R. Coifman, V. Rokhlin, and S. Wandzura, (1993)]. Thus, the
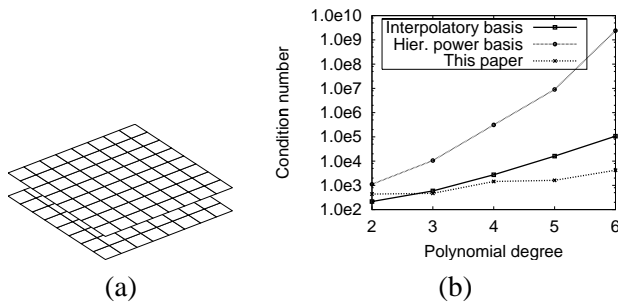
Figure 3 : Condition number of the EFIE implemented using different higher-order basis functions (Interpolatory [R. D. Graglia, D. R. Wilton, and A. F. Peterson, (1997)] and hierarchical power basis [B. M. Kolundzija and B. Popovic, (1993)]).

MLFMM plays a most important role in the solution algorithm, and its parallelization is essential in porting the FE-BI or VIE solvers to distributed computing platforms.

In considering the parallelization of the matrix-vector products in the MLFMM algorithm, we must examine the three basic steps within the algorithm: (1) the radiation, or signature functions of each group at the $(n+1)^{th}$ level aggregated to form the radiation functions of the parent groups, i.e. groups at the $(n)^{th}$ level; (2) the translation of the radiation functions to cluster centers located in the far-zone of the source cluster at the $(n)^{th}$ level, provided their parents at the $(n-1)^{th}$ level are in the near-zone of each other; (3) the disaggregation step, where the children clusters at the $(n+1)^{th}$ level are disaggregated to compute the fields within the clusters. These three steps are depicted in Fig. 4 for a three-level FMM tree. A successful parallel implementation of these three steps requires

- Careful balancing of the computational load among the processors, and

- Minimal communication between the processors.

Load balancing requires the distribution of the MLFMM tree structure on the nodes of the parallel process. For the sake of simplicity, let us consider the tree structure given in Fig. 4, consisting of 2 main clusters at the coarsest level. If the tree is distributed on 2 nodes of a parallel process, assuming that each cluster at each level has the same number of far-zone clusters, we would achieve a perfectly balanced distribution. For such a case, the aggregation and disaggregation steps can be carried out on

separate processors independently, without interprocessor communication. The only required communication will take place at the translation step when the source and target clusters lie on different processors. However, this requires a significant amount of communication between processors, as will be explained below. With vector processing capabilities on computing platforms, the actual work at the translation step on each processor is quite small and comparable to the time used for communication. Consequently, communication among processors becomes a bottleneck for the parallel performance of the MLFMM implementation.
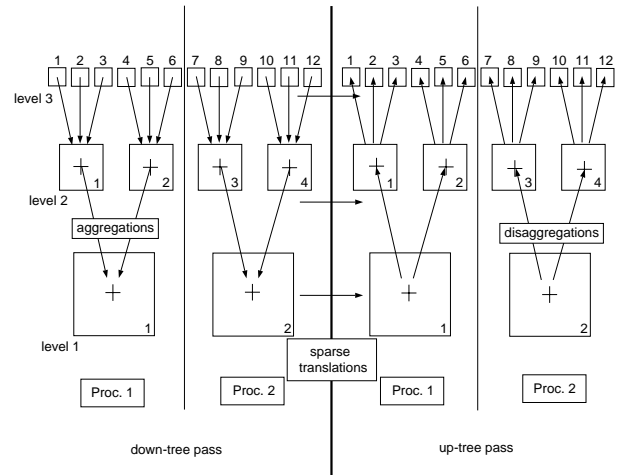

Figure 4 : A hypothetical MLFMM clustering tree.

To better explain the situation, let us assume that at the 1st level, clusters 1 and 2 are in the near-zone of each other. Furthermore, let us assume that at the 2nd level, clusters 1 and 2 are in the near-zone of each other (similarly, clusters 2 and 3 and clusters 3 and 4 are in the near-zone of each other) and clusters 3 and 4 lie in the far-zone of cluster 1 and clusters 1 and 2 lie in the far-zone of cluster 4. Likewise, at the 3rd level, clusters 1 to 3 lie in the near-zone of each other and clusters 4 to 12 lie in the far-zone of clusters 1 to 3, and so on. Each processor can independently compute the aggregations at all levels starting from level 3 (we'll call this the down-tree pass). Likewise, once the pertinent data is available, the disaggregations at all levels can be computed on separate processors, independently (up-tree pass). However, interprocessor communication is necessary for the translation operations since, for example, clusters 1 and 3 (at level 2) lie on different processors and the translation operation
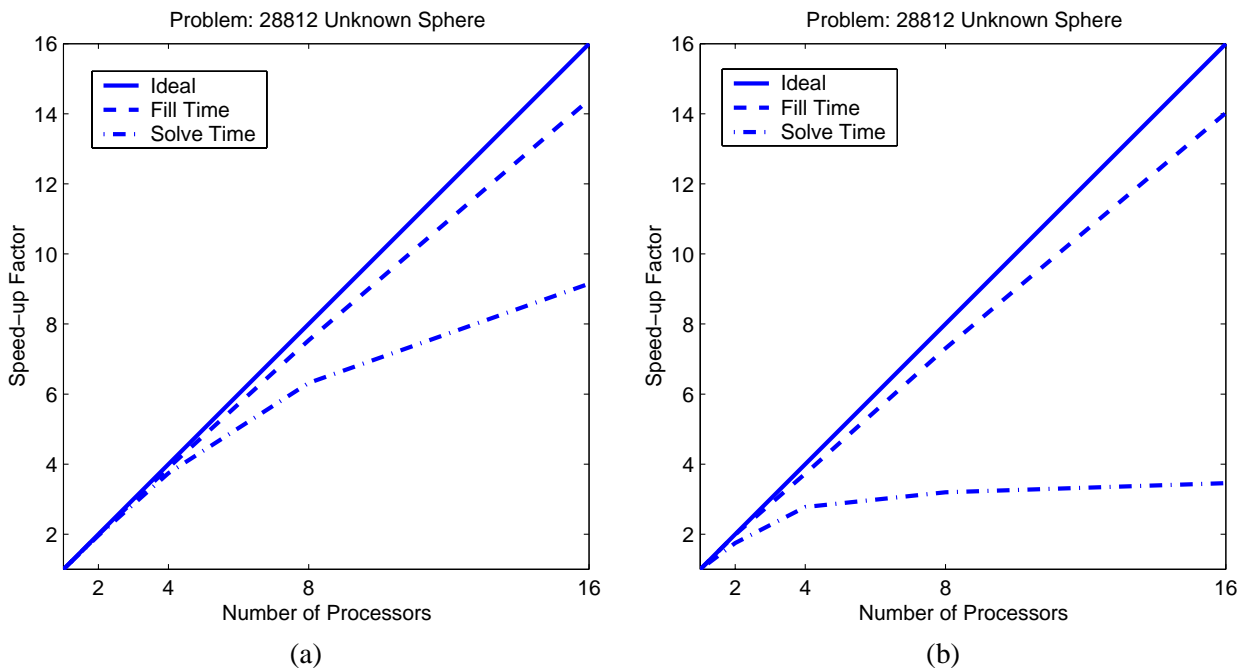
Figure 5 : Performance of parallel MLFMM for a 28,812 unknown sphere, (a) no compiler optimizations, (b) –O4 compiler optimizations

requires the radiation function of cluster 1 to be translated onto cluster 3. For level 2, the required number of operations for the translation step is $3 \times 2L_2^2$ per processor. Thus the length of data that must be communicated between processors is $3 \times 2L_2^2$ in each direction. For level 3 the situation is slightly different. If we had assumed that clusters 2 and 3 at level 2 were in the near-field of each other, we would need to execute $2 \times 3 \times 3 \times 2L_3^2$ operations to evaluate the translated fields between the children of cluster 2 and 3 (at level 2). This simple example demonstrates the high rate of inter-processor communication needed at the translation step of the MLFMM algorithm. Via aggressive optimization in compiling the MLFMM code on computers with vector processing capabilities, the intra-processor work load can be significantly reduced. Hence, the inter-processor communication speed remains a bottleneck for optimal performance of the MLFMM on distributed memory parallel computers. Below, we present some preliminary performance data and point out the effects of inter-processor communication speed.

As an example, consider the scattering by a sphere of 1m. radius. A balanced MLFMM grouping leads to 5 MLFMM levels each with 8, 56, 272, 1157, and 4517 non-empty cubes. For parallelization, this tree is dis-

tributed among processors on the basis of second level clusters, and the performance test was carried out on an IBM SP3 computer having three nodes, each with eight, 375 MHz Power3 processors ($3 \times 8 = 24$ processors). The high-speed switch connecting the three nodes can deliver 500 MB/s bi-directionally to each processor. Both the matrix-fill and the iterative solution time were recorded to evaluate performance. Parallelization of the near-field matrix is straightforward and will not be discussed here.

Specifically, we show the parallel performance for a 1 m radius sphere at 0.75 GHz. This problem resulted in 28,812 unknowns and as seen in Fig. 5, severe performance deterioration is observed due to inter-processor communication. For the non-optimized code, better parallelization performance is observed since the evaluation of the translations has a significant computational burden at this step. However, for the optimized code (–O4 option), the inter-processor communication dominates after the 4th processor is added, leading to saturation. We note here that, for a serial run (single processor), the matrix fill time demonstrated a speed-up factor of 3.7, whereas the solution time was 8.2 times faster after compiler optimizations. In light of the above observations, we conclude that even for a very well balanced problem, inter-
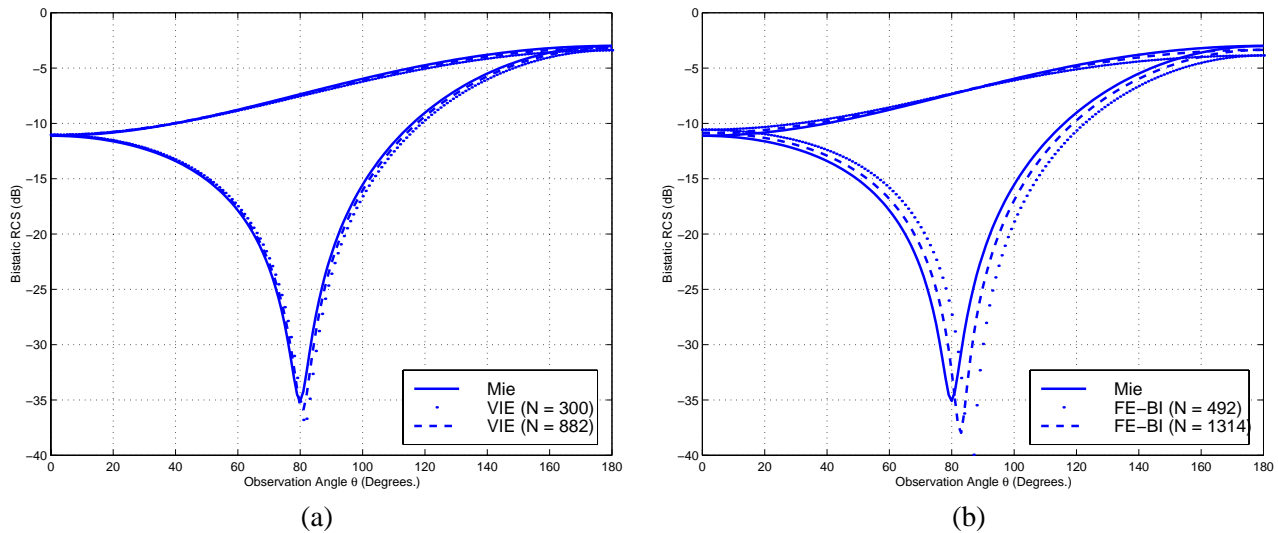
Figure 6 : Bistatic RCS of a dielectric sphere of radius 0.2λ ($\varepsilon_r = 2.592$). (a) VIE Solution, (b) FE-BI Solution

processor communication remains the bottleneck for the parallel performance of MLFMM on distributed memory computers. Consequently, future efforts must focus on significant re-organization of the MLFMM algorithm for massively distributed platforms.

6 Comparison Data Between VIE and FE-BI Formulation

To validate the proposed VIE for magnetic materials, we consider a comparison of the scattering by a sphere (canonical problem) and a cube. A secondary goal is to provide an initial comparison of the solution performance for the VIE and FE-BI methods for these specific structures.

The considered sphere example refers to a purely dielectric problem. The sphere radius is 0.2λ and $\varepsilon_r = 2.592$. As depicted in Fig. 6, the bistatic radar cross section (RCS) patterns calculated using the FE-BI and VIE methods are in excellent agreement with the exact Mie series data. However, the FE-BI required more unknowns to achieve the same accuracy. Thus, to better compare the VIE and FE-BI methods, we consider a comparison of the solution error vs. the element's edge length (in both cases the same curvilinear hexahedra were used). This comparison was done for the sphere example and resulted in the curves given in Fig. 7. These depict that the error is proportional to the square of the element's edge length for both methods. However, the VIE can afford larger elements for the same error ($\Delta_{VIE} \approx \sqrt{2}\Delta_{FE-BI}$). Also, as shown in Tab. 2, the VIE system converges much
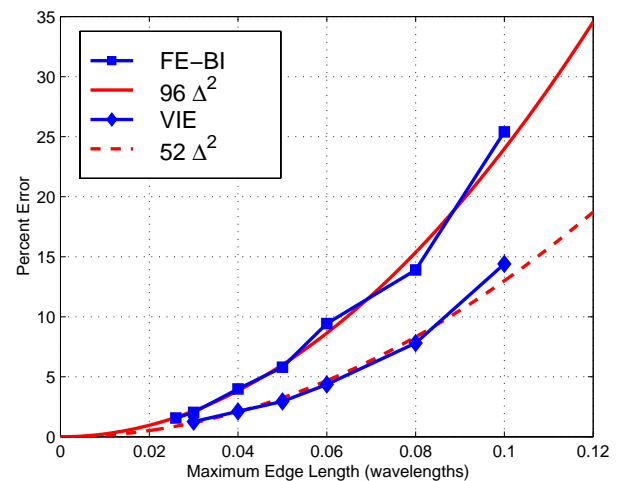

Figure 7 : Convergence curves of the FE-BI and VIE solvers with respect to maximum edge length.

faster but the matrix fill time is significantly higher for the VIE formulation. The latter is a clear disadvantage of the VIE method, but the rapid convergence of its associated matrix system provides incentives for further examination of the method. Clearly, this comparison refers to a specific example and should not be generalized at this stage. Most likely, the FE-BI method will be a choice method for many composite structures but the VIE offers advantages that should be further examined. Suitable preconditioning methods could also play a major role in the efficiency of each method (as is the case for the array example).
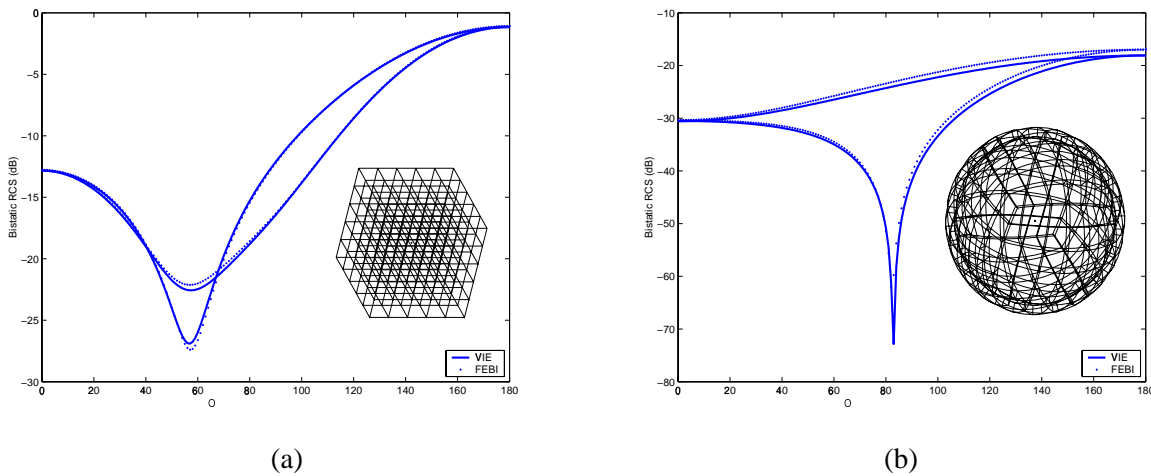
(a)   (b)

Figure 8 : Bistatic RCS of two magneticly perpeable scatterers, (a) A cube of side length 0.5λ and $\mu_r = 2.2$, (b) A spherical shell of $\mu_r = 2.2$, 0.2λ outer radius, and 0.18λ inner radius.

Table 2 : Performances of VIE and FE-BI formulations for the sphere.

	Number of Unknowns	Matrix Fill Time (s.)	Number of Iterations	Time per per Solution (s.)
VIE	300	107	11	0.41
VIE	882	1211	13	5.00
FE-BI	492	1.3	160	4.08
FE-BI	1314	6.3	354	50.14

Figure 9 : Tapered Slot Antenna Element

We next consider the scattering (plane wave incidence is normal to the cube's face) by a permeable cube. To our knowlegde, this is the first published implementation of the VIE for magnetic volumes. The specific cube has a side length of 0.5λ and $\mu_r = 2.2$. As seen, the VIE and FE-BI data are in good agreement and demonstrate the validity of Eq. (5). Also shown in Fig. 8 (b) is the radar scattering by a spherical shell having an outer radius of 0.2λ, an inner radius of 0.18λ, and a relative permeability of $\mu_r = 2.2$. Again, the comparison between the FE-BI and VIE data is excellent.

We conclude this section by presenting the radiation of a large $30 \times 30 = 900$ element rectangular array of tapered slot antennas (TSAs) (see Fig. 9 for the element geometry). The discretization of this element resulted in 1103 unknowns (506 FE and 596 BI unknowns) leading to nearly a million unknowns for the entire matrix system (992,700 unknowns).
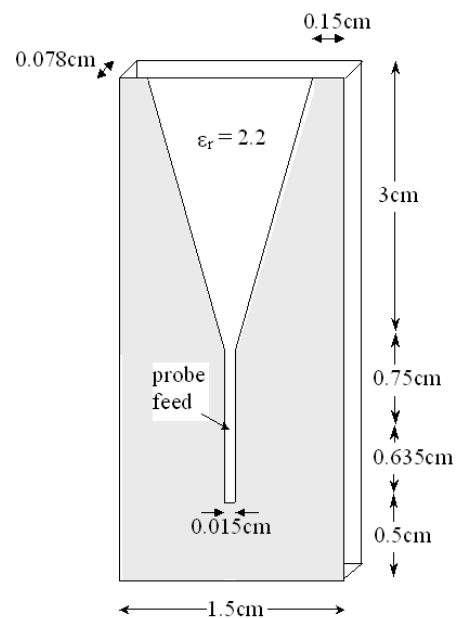
By using the proposed decomposition method (system reconstructing) illustrated in Fig. 2, the storage alone was reduced from 3.8 terabytes down to 16GBytes, and could thus be solved. Moreover, the solution time was only 18.6 hours, a reduction by 3 orders of magnitude as compared to a conventional FE-BI implementation. Thus, realistic finite arrays can be evaluated and designed using the proposed decomposition method. As an example, Fig. 10 shows the field distribution and corresponding array pattern for a 16×16 TSA array with 20 dB Taylor
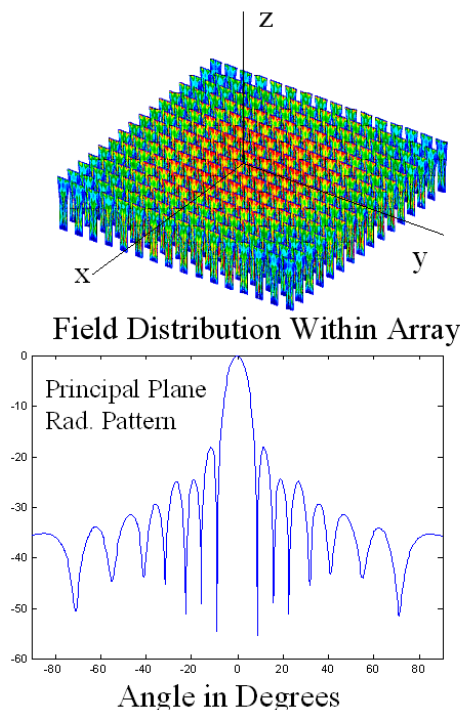
tapering ($\overline{n} = 4$).

Figure 10 : Field distribution and radiation pattern of a 16×16 TSA array with 20 dB. Taylor tapering ($\overline{n} = 4$).

7   Conclusions

Recent developments on fast solution algorithms and on-going advances in computer technology has allowed the solution of realistic scattering and radiation problems involving hundreds of thousands of unknowns on personal computers in a few hours. Nevertheless, large-scale problems involving the simulation of full-scale vehicles at X-band frequencies still place extensive demands on the performance of available fast algorithms. For such large-scale problems, one must inevitably resort to high performance, multiprocessor computing platforms to allow for multi-spectral and multi-angle evaluations. The situation is even more stressing when volumetric material structures are considered along with metallic surfaces. Needless to mention, there is a necessity for well conditioned systems and for high geometrical fidelity to generate accurate solutions of large scale problems.

In this paper we discussed progress on several topics relating to fast integral methods and their application in modeling composite and volumetric material structures. Among them, we introduced volumetric modeling of magnetic materials using VIE methods and compared results with data based on the FE-BI technique. We also discussed preconditioning, parallelization of the MLFMM and volumetric basis functions for curvilinear hexahedra (based on covariant mapping to maintain tangential vector continuity and leading to contravariant projection edge-based basis functions). The latter, have the desirable property of vanishing divergence within the element but non-zero curl. In addition, a new domain decomposition is introduced for large array evaluations involving several million degrees of freedom and using resources which are three orders of magnitude smaller.

References

Andersen, L. S.; Volakis, J. L. (1999):   Development and application of a novel class of hierarchical tangential vector finite elements for electromagnetics. *IEEE Trans. Antennas Propagat.*, vol. 47, pp. 104–108.

Antilla, G. E.; Alexopoulos, N. G. (1994):   Scattering from complex 3d geometries by a curvilinear hybrid finite element-integral equation approach. *J. Opt. Soc. Am. A.*, vol. 11, no. 4, pp. 1445–1457.

Castillo, P.; Koning, J.; Rieben, R.; White, D. (2003):   A discrete differential forms framework for computational electromagnetism. *CMES: Computer Modeling in Engineering & Sciences*, vol 5, no. 4, pp. 331–346.

Chew, W. C.; Jin, J.-M.; Michielssen, E.; Song, J. ed., (2001):   *Fast and Efficient Algorithms in Computational Electromagnetics.* Artech House.

Chew, W. C.; Song, J. M.; Cui, T. J.; Velamparambil, S.; Hastriter, M. L.; Hu, B. (2003):   Review of large scale computing in electromagnetics with fast integral equation solvers. *CMES: Computer Modeling in Engineering & Sciences*, vol 5, no. 4, pp. 361–372.

Coifman, R.; Rokhlin, V.; Wandzura, S. (1993):   The fast multipole method for the wave equation: a pedestrian prescription. *IEEE Antennas and Propagat. Mag.*, vol. 35, pp. 7–12.

Graglia, R. D.; Uslenghi, P. L. E.; Zich, R. S. (1989): Moment method with isoparametric elements for three-dimensional anisotropic scatterers. *Proc. IEEE*, vol. 77, no. 5, pp. 750–760.

Graglia, R. D.; Wilton, D. R.; Peterson, A. F. (1997): Higher order interpolatory vector bases for computational electromagnetics. *IEEE Trans. Antennas Propagat.*, vol. 45, no. 3, pp. 329–342.

Harrington, R. F. (1968): *Field computation by moment methods*. Macmillan.

Jin, J.-M.; Volakis, J. L.; Liepa, V. V. (1989): A moment method solution of a volume-surface integral equation using isoparametric elements and point matching (te scattering). *IEEE Trans. Microwave Theory Tech.*, vol. 37, no. 10, pp. 1641–1645.

Jorgensen, E.; Volakis, J. L.; Meincke, P.; Breinbjerg, O. (2002): Higher-order hierarchical legendre basis functions for iterative integral equation solvers with curvilinear surface modeling. *IEEE International Symposium on Antennas and Propagation, San Antonio, TX., Digest*, pp. 618–621.

Kindt, R. W.; Sertel, K.; Topsakal, E.; Volakis, J. L. (2003): Array decomposition method for the accurate analysis of finite arrays. *IEEE Trans. Antennas Propagat.*, vol. 51, no. 6, pp. 1364-1372.

Kolundzija, B. M.; Popovic, B. (1993): Entire-domain galerkin method for analysis of metallic antennas and scatterers. *IEE Proc.-H*, vol. 140, no. 1, pp. 1–10.

Livesay, D. E.; Chen, K. (1974): Electromagnetic fields induced inside arbitrarily shaped biological bodies. *IEEE Trans. Microwave Theory Tech.*, vol. 22, pp. 1273–1280.

Peterson, A. F.; Wilton, D. R. (1996): *Finite Element Software in Microwave Engineering, Ch. 5*. Edited by Pelosi and Silvester, Italy: Wiley-InterScience.

Peterson, A. F. (1998): Analysis of heterogeneous electromagnetic scatterers: research progress of the past decade. *Proc. IEEE*, vol. 79, no. 10, pp. 1431–1441.

Poggio, A. J. (1973): *Integral equation solutions of three dimensional scattering problems in Computer Techniques for Electromagnetics*. Oxford, U.K.: Permagon.

Richmond, J. H. (1965): Scattering from a dielectric cylinder of arbitrary cross section shape. *IEEE Trans. Antennas Propagat.*, vol. 13, pp. 334–341.

Saad, Y. (1996): *Iterative Methods for Sparse Linear Systems*. Boston: PWS Pub. Co.

Schaubert, D. H.; Wilton, D. R.; Glisson, A. W. (1984): A tetrahedral modeling method for electromagnetic scattering by arbitrarily shaped inhomogeneous dielectric bodies. *IEEE Trans. Antennas Propagat.*, vol. 32, no. 1, pp. 77–85.

Sertel, K.; Volakis, J. L. (2000): Incomplete lu preconditioner for fmm implementation. *Microwave Opt. Tech. Lett.*, vol. 26, no. 7, pp. 265–267.

Sertel, K.; Volakis, J. L. (2002): Method of moments solution of volume integral equations using parametric geometry. *Radio Sci.*, vol. 37, no. 1, pp. 1–7.

Volakis, J. L. (1992): Alternative field representations and integral equations for modeling inhomogeneous dielectrics. *IEEE Trans. Microwave Theory Tech.*, vol. 40, no. 3, pp. 604–608.

Volakis, J. L.; Ozdemir, T.; Gong, J. (1997): Hybrid finite-element methodologies for antennas and scattering. *IEEE Trans. Antennas Propagat.*, vol. 45, no. 3, pp. 493–507.

Volakis, J. L.; Chatterjee, A.; Kempel, L. (1998): *Finite Element Methods for Electromagnetics*. IEEE Press, New York.

Volakis, J. L.; Eibert, T. F.; Sertel, K. (2000): Fast integral methods for conformal antenna and array modeling in conjunction with hybrid finite element formulations. *Radio Sci.*, vol. 35, no. 2, pp. 537–546.

Webb, J. P. (1999): Hierarchical vector basis functions of arbitrary order for triangular and tetrahedral finite elements. *IEEE Trans. Antennas Propagat.*, vol. 47, no. 8, pp. 1244–1253.

Appendix A: Basis Functions for VIEs

The application of higher-order hexahedral elements given in [G. E. Antilla and N. G. Alexopoulos, (1994)] is extended to the VIE formulation. The geometry is discretized using parametric hexahedra defined by 27 points on a topologically rectangular grid in space as depicted in Fig. 11. Any point inside the hexahedron is a parametric mapping of a corresponding point in the unit cube in the parameter space through the transformation

$$\mathbf{r}(u,v,w) = \sum_{i=0}^{2}\sum_{j=0}^{2}\sum_{k=0}^{2}\mathbf{r}_{ijk}L_{ijk}(u,v,w)$$
$$for \quad (u,v,w) \in ([0,1],[0,1],[0,1]) \qquad (19)$$

where $\mathbf{r}_{ijk}$ are the defining 27 points of the hexahedron and $L_{ijk}(u,v,w)$ are the quadratic Lagrange interpolation polynomials in three parameters (u,v,w). These coefficients can be constructed using the 27 constraints: $\mathbf{r}(0.0,0.0,0.0) = \mathbf{r}_{000}$, $\mathbf{r}(0.5,0.0,0.0) = \mathbf{r}_{100}$, $\mathbf{r}(1.0,0.0,0.0) = \mathbf{r}_{200}$, ..., $\mathbf{r}(1.0,1.0,1.0) = \mathbf{r}_{222}$.
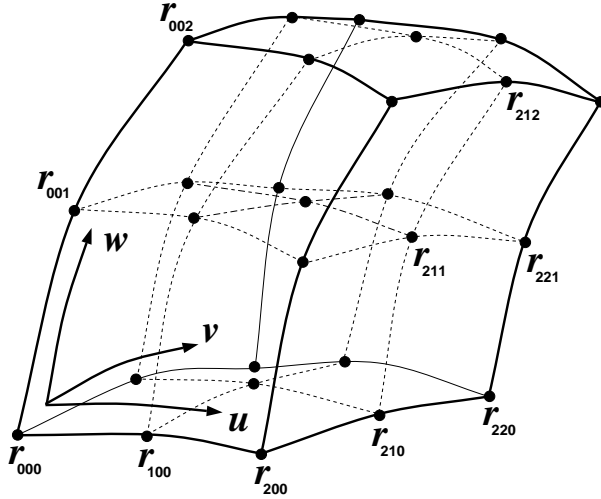

Figure 11 : Curvilinear hexhahedral element.

The set of basis functions used in this work are edge based functions defined in curved hexhedra, identical to those used in [G. E. Antilla and N. G. Alexopoulos, (1994)]. However, for VIE implementation, our edge-based basis functions are defined in terms of the covariant unitary basis vectors. Specifically, the four basis functions associated with the edges parallel to the parametric direction u have the form (referred to as contravariant projection form)

$$\mathbf{e}^{(u)}(\mathbf{r}) = \frac{1}{\sqrt{G}} \left\{ \begin{array}{c} 1-v \\ v \end{array} \right\} \left\{ \begin{array}{c} 1-w \\ w \end{array} \right\} \mathbf{a}_u. \qquad (20)$$

Similarly, for the edges in the v and w parametric directions, the basis functions are defined as

$$\mathbf{e}^{(v)}(\mathbf{r}) = \frac{1}{\sqrt{G}} \left\{ \begin{array}{c} 1-u \\ u \end{array} \right\} \left\{ \begin{array}{c} 1-w \\ w \end{array} \right\} \mathbf{a}_v, \qquad (21)$$

$$\mathbf{e}^{(w)}(\mathbf{r}) = \frac{1}{\sqrt{G}} \left\{ \begin{array}{c} 1-u \\ u \end{array} \right\} \left\{ \begin{array}{c} 1-v \\ v \end{array} \right\} \mathbf{a}_w. \qquad (22)$$

Here, G is the determinant of the parametric transformation in Eq. (19):

$$G = \begin{vmatrix} g_{uu} & g_{uv} & g_{uw} \\ g_{vu} & g_{vv} & g_{vw} \\ g_{wu} & g_{wv} & g_{ww} \end{vmatrix} \qquad (23)$$

in which

$$g_{\eta\xi} = \mathbf{a}_\eta \cdot \mathbf{a}_\xi \qquad (24)$$

where η and ξ represent any pair of the parameters u, v, and w, and $\mathbf{a}_\eta = \frac{\partial \mathbf{r}}{\partial \eta}$. Together, $\mathbf{e}^{(u)}$, $\mathbf{e}^{(v)}$, $\mathbf{e}^{(w)}$ constitute a set of 12 basis functions for each hexahedron. The total number of unknowns for a given tessellation is determined by the number of edges in the mesh, since the coefficients of basis functions in neighboring elements are associated with the same edge (i.e. an edge shared by 2 or more hexahedra). Thus, $\mathbf{e}_i$ in Eq. (6) will be some combination of Eq. (20)-Eq. (22) from different hexahedra as determined by the impedance matrix assembly process.

The basis functions defined here are slightly different from those given in [G. E. Antilla and N. G. Alexopoulos, (1994)]. They are defined in terms of covariant unitary basis vectors, whereas the basis functions in [G. E. Antilla and N. G. Alexopoulos, (1994)] are defined using contravariant unitary basis vectors. Being defined by covariant basis vectors, they have the advantage of having zero divergence

$$\nabla \cdot \mathbf{e} = \frac{1}{\sqrt{G}} \left\{ \frac{\partial}{\partial u}(\mathbf{e} \cdot \mathbf{a}^u \sqrt{G}) + \frac{\partial}{\partial v}(\mathbf{e} \cdot \mathbf{a}^v \sqrt{G}) \right. \\ \left. + \frac{\partial}{\partial w}(\mathbf{e} \cdot \mathbf{a}^w \sqrt{G}) \right\} \quad (25)$$

inside the hexahedron (this is not true for the basis functions in [G. E. Antilla and N. G. Alexopoulos, (1994)]). This is a property that must be satisfied by the electric field intensity $\mathbf{E}$. In Eq. (25), the contravariant unitary vectors are defined as

$$\mathbf{a}^u = \frac{1}{\sqrt{G}}(\mathbf{a}_v \times \mathbf{a}_w),$$

$$\mathbf{a}^v = \frac{1}{\sqrt{G}}(\mathbf{a}_w \times \mathbf{a}_u),$$

$$\mathbf{a}^w = \frac{1}{\sqrt{G}}(\mathbf{a}_u \times \mathbf{a}_v). \qquad (26)$$

Evaluation of this curl operation can be readily carried out for a covariant projection. Namely, if a general vector is expressed as

$$\mathbf{e} = (\mathbf{e} \cdot \mathbf{a}_u)\mathbf{a}^u + (\mathbf{e} \cdot \mathbf{a}_v)\mathbf{a}^v + (\mathbf{e} \cdot \mathbf{a}_w)\mathbf{a}^w \qquad (27)$$

its curl is given by

$$
\begin{aligned}
\nabla \times \mathbf{e} \; = \; & \frac{1}{\sqrt{G}} \left\{ \left[\frac{\partial(\mathbf{e} \cdot \mathbf{a}_w)}{\partial v} - \frac{\partial(\mathbf{e} \cdot \mathbf{a}_v)}{\partial w} \right] \mathbf{a}_u \right. \\
& + \left[\frac{\partial(\mathbf{e} \cdot \mathbf{a}_u)}{\partial w} - \frac{\partial(\mathbf{e} \cdot \mathbf{a}_w)}{\partial u} \right] \mathbf{a}_v \\
& + \left. \left[\frac{\partial(\mathbf{e} \cdot \mathbf{a}_v)}{\partial u} - \frac{\partial(\mathbf{e} \cdot \mathbf{a}_u)}{\partial v} \right] \mathbf{a}_w \right\}.
\end{aligned}
\tag{28}
$$

Since the basis functions used here are defined in contravariant projection form, the evalution of Eq. (28) is rather lengthy, involving derivatives of G and $\mathbf{a}_\eta$, ($\eta = u, v, w$).